Macromolecules

pubs.acs.org/Macromolecules

Article

Salt-Mediated Tuning of the Cononsolvency Response Behavior of PNIPMAM Thin Films

Julija Reitenbach, Peixi Wang, Linus F. Huber, Simon A. Wegener, Robert Cubitt, Dirk Schanzenbach, André Laschewsky, Christine M. Papadakis, and Peter Müller-Buschbaum*

Cite This: *Macromolecules* 2024, 57, 10635−10647

Read Online

ACCESS | Metrics & More | Article Recommendations | Supporting Information

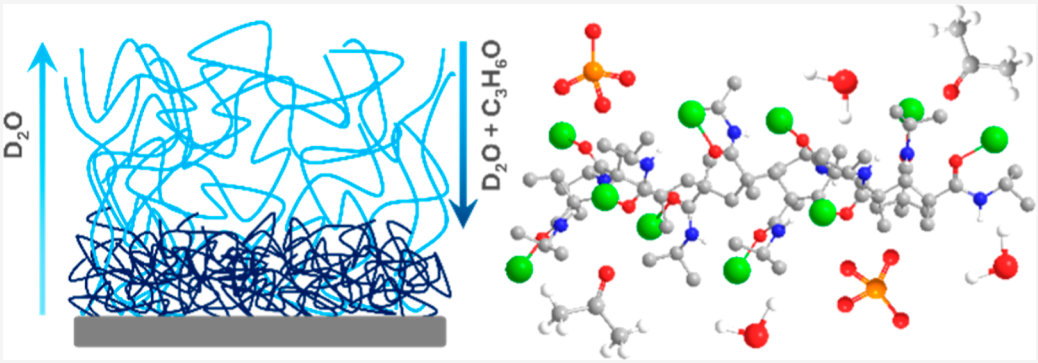

ABSTRACT: The development of tuning parameters to influence the response behavior of polymer-based nanodevices is investigated by the addition of $NaClO_4$ or $Mg(ClO_4)_2$ to adjust the swelling degree of poly(*N*-isopropylmethacrylamide) thin films under different vapor atmospheres. By leveraging the cononsolvency effect of the polymer in a mixed vapor of water and acetone, a contraction of the preceding water-swollen films is induced. The relation between the macroscopic and the molecular processes is elucidated by static and time-resolved time-of-flight neutron reflectometry, as well as by in situ Fourier transform infrared spectroscopy. It is found that the addition of $NaClO_4$ strongly enhances the film thickness response for swelling and contraction, which, therefore, allows the tuning of the film toward stronger responses. Mechanistically, D_2O−amide bonds are formed during swelling and become perturbed upon vapor exchange. Thereby, the D_2O−amide interactions are reduced continuously, while acetone−amide interactions develop, accompanied by increasing amide−amide interactions during the film contraction.

INTRODUCTION

Amidst the various types of stimuli-responsive materials,[1−3] thermoresponsive polymers have attracted particular attention.[4−7] Characteristically, the temperature-induced changes in their hydrophilicity can be translated into a coil-to-globule collapse transition that dramatically affects their water solubility and aggregation behavior. Mostly, two different scenarios are exploited. Either the polymer becomes soluble with increasing temperature, for which the related transition is characterized by an upper critical solution temperature (UCST), or the polymer becomes insoluble at higher temperatures, and the resulting phase transition is characterized by a lower critical solution temperature (LCST).[8−10] The driving force behind the thermoresponsivity of polymers reflects the thermodynamical preference of interactions between the polymer and the solvent molecules compared to the sum of interactions between the polymer chains and between the solvent molecules themselves.[11−13] Besides depending on the intrinsic features of the polymer, such as molar mass, tacticity, and end groups, the transition temperature can be modified by additives that modulate the inter- and intramolecular interactions.[14−17] In certain cases, adding an organic cosolvent, which is also a good solvent for the polymer, can lead to a variation of the LCST with a distinct minimum at a certain composition of the solvent mixture.[18−21] At a given temperature, a miscibility gap is observed for a certain range of compositions of the solvent mixture. This intriguing phenomenon is known as the cononsolvency effect, for which the detailed origins are still under debate.[19,21,22] The theories put forward range from explanations based on intrinsic properties to preferential interactions between specific constituents of the system.[23−32] In addition to theoretical studies and computer simulations, experimental investigations allow us to obtain insights into influencing factors, and a

Received: August 28, 2024
Revised: October 23, 2024
Accepted: October 29, 2024
Published: November 8, 2024

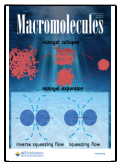

https://doi.org/10.1021/acs.macromol.4c02053
Macromolecules 2024, 57, 10635−10647

number of different polymers, cosolvents, and sample architectures have been investigated.[20,24,33−41] To further leverage the cononsolvency effect in devices, polymers in thin film geometry are attractive candidates due to their fast response, mechanical stability, and easy fabrication compared to polymers in solution or polymer brushes.[42,43] Most of the reported cases concern polymers in aqueous media and have been carried out on the same polymer, namely, poly(*N*-isopropylacrylamide) (PNIPAM). Structurally related to the well-studied PNIPAM is poly(*N*-isopropylmethacrylamide) (PNIPMAM), which in aqueous solution not only shows LCST type II behavior like PNIPAM but also exhibits a cononsolvency effect in a number of solvent mixtures.[20,33,41,44−48] Furthermore, in thin film geometry, PNIPMAM is amorphous and has a high water-uptake ability, and due to the additional methyl group on the backbone, PNIPMAM thin films feature a higher glass transition temperature and are more resistant to hydrolysis.[20] In previous studies, it was found that for diblock copolymer thin films consisting of a short poly(methyl methacrylate) (PMMA) and a PNIPAM[40] or a PNIPMAM block[45] strong deviations in the response behavior toward different vapor atmospheres occur, despite the difference in only a methyl group in the polymer backbone. For the PMMA-*b*-PNIPMAM thin films, an overall stronger increase in film thickness upon water vapor atmosphere exposure was obtained as well as a pronounced, abrupt contraction under exchange to a water−acetone vapor atmosphere. Since hydrogel-based devices rely on detection mechanisms that have to adapt to the volume or weight of the thin polymer film, a fast and strong response to an external trigger is crucial.[49] To circumvent the laborious tailored synthesis of new polymers, which specifically meet the requirements imposed by the respective application, the ability to modify the response behavior of already established polymers, such as simple homopolymers, will be very valuable. It is known that specific ion effects impact various phenomena, such as solvent interactions or the LCST of thermoresponsive polymers.[14,50−53] In this regard, the addition of salts in the fabrication process of polymer thin films should provide an easy route to tuning the response behavior of polymer thin films.

In the present study, the cononsolvency behavior of PNIPMAM homopolymer thin films is modulated with the addition of two different perchlorate salts, namely, $NaClO_4$ and $Mg(ClO_4)_2$. As demonstrated previously,[54] adding a Mg salt with a chaotropic anion enables the modification of the swelling behavior of PNIPMAM thin films in a D_2O vapor atmosphere. In the present study, $NaClO_4$ and $Mg(ClO_4)_2$ are chosen on the one hand to be able to make comparisons to our previous study and to, on the other hand, have a more chaotropic cation in the form of Na^+. Therefore, here the influence of the cation is analyzed, and the investigation of tuning not only the swelling but also the collapse response is motivated. The cononsolvency effect of PNIPMAM hydrogel films is induced by switching from a pure D_2O vapor atmosphere to a mixed D_2O−acetone vapor atmosphere with a volume-to-volume ratio of 9:1, which was known to induce the cononsolvency effect in PNIPMAM-based diblock copolymers.[45,48] The evolution of the thickness and the solvent content inside the thin films is investigated by time-of-flight neutron reflectometry (ToF-NR). In addition, in situ Fourier transform infrared spectroscopy (FTIR) measurements are conducted to obtain insights into the solvation processes of the individual components. The sequence of solvation events is further determined by the analysis of selected FTIR bands to provide further understanding of the complex kinetic processes during water uptake and cosolvent-induced water release.

EXPERIMENTAL SECTION

Materials. 2,2,2-Trifluoroethanol (CF_3CH_2OH, ReagentPlus, ≥99%), acetone (C_3H_6O, ACS reagent, ≥99.5%), magnesium perchlorate ($Mg(ClO_4)_2$, ACS reagent), and sodium perchlorate ($NaClO_4$, ACS reagent, ≥98.0%) were purchased from Sigma-Aldrich. Sulfuric acid (H_2SO_4, 95−98%), hydrogen peroxide (H_2O_2, 30% aq.), and hydrophobic poly(tetrafluoroethylene) (PTFE) filters (pore size: 0.45 μm) were received from Carl Roth GmbH. Deuterated water (D_2O, 99.95%) was purchased from Deutero GmbH (Kastellaun, Germany). A Milli-Q Plus purification system from Merck Millipore (Burlington, U.S.A.) was used to obtain deionized water with a resistivity of 18.2 $M\Omega cm^{-1}$. Silicon wafers (p/Bor, ⟨100⟩, d = 525 ± 25 μm, 10−20 Ωcm) were purchased from Si-Mat (Kaufering, Germany).

Polymer Synthesis. The PNIPMAM homopolymer was synthesized via conventional free radical polymerization as described previously.[54]

Sample Preparation. The preparation of X-ray reflectometry (XRR), grazing incidence small-angle X-ray scattering (GISAXS), ToF-NR, and FTIR samples is described in the Supporting Information.

Methods. *X-ray Reflectometry (XRR).* XRR measurements were performed on a D8 Advance diffractometer (Bruker, Billerica). The data was analyzed by using the Python program *refnx*.[55] Details are provided in the Supporting Information. To describe the reflectivity curves and to obtain the X-ray scattering length density (SLD) profiles of the salt-containing PNIPMAM thin films, a three-layer model was applied consisting of, apart from a silicon layer with its native oxide layer for the substrate as well as infinite air at the top of the sample, a polymer−substrate interface, a polymer bulk layer, and a polymer−air interface. The X-ray SLD values of the salts were calculated according to literature[57] as 18.71 × 10^{-6} $Å^{-2}$ for $Mg(ClO_4)_2$ and 21.03 × 10^{-6} $Å^{-2}$ for $NaClO_4$. The SLD values for H_2O and acetone are 9.47 × 10^{-6} and 7.36 × 10^{-6} $Å^{-2}$, respectively.[57] The SLD of PNIPMAM was calculated as 10.37 × 10^{-6} $Å^{-2}$.[57] Detailed fit results are given in Table S1 in the Supporting Information.

Grazing Incidence Small-Angle X-ray Scattering (GISAXS). GISAXS measurements were performed with a Ganesha SAXSLAB laboratory X-ray instrument. Details are provided in the Supporting Information.

Time-of-Flight Neutron Reflectometry (ToF-NR). ToF-NR measurements were performed at the Institute Laue-Langevin (ILL) in Grenoble, France, using instrument D17. More details are provided in the Supporting Information. The samples were mounted vertically into a 3D-printed, custom-made chamber to be free-standing.[56] The temperature was kept constant at T = 23 °C. The neutron SLD values of the added salts were calculated according to literature[57] as 4.23 × 10^{-6} $Å^{-2}$ for $Mg(ClO_4)_2$ and 4.48 × 10^{-6} $Å^{-2}$ for $NaClO_4$. The SLD values for H_2O, D_2O, and acetone are −0.56 × 10^{-6}, 6.39 × 10^{-6}, and 0.27 × 10^{-6} $Å^{-2}$, respectively.[57] The SLD of PNIPMAM was calculated as 0.74 × 10^{-6} $Å^{-2}$.[57] In general, the same conceptual design of the layer model as for the XRR analysis was used, and the fits were performed using the Python program *refnx*.[55] For static ToF-NR data, interface layers were not included if reasonable agreement between the fit and the data was achieved. Details about the exact layer structure for each static ToF-NR analysis are given in Table S2 in the Supporting Information. The time-resolved ToF-NR data was fitted using a single layer to describe the salt-containing polymer bulk apart from a silicon layer with its native oxide layer for the substrate as well as infinite air at the top of the sample. Interface layers are not included in the analysis of kinetic ToF-NR data due to the narrow q-range selected to enable a high time resolution.

https://doi.org/10.1021/acs.macromol.4c02053
Macromolecules 2024, 57, 10635−10647

Fourier Transform Infrared Spectroscopy (FTIR). FTIR measurements were performed using an Equinox 55 (Bruker Optik GmbH, Rosenheim, Germany) spectrometer, as described in detail in the Supporting Information. The samples were placed vertically into a closable and temperature-controllable copper chamber.

2D FTIR Correlation Analysis. 2D FTIR correlation analysis was performed according to the Python analysis script provided by Morita (Kwansei-Gakuin University, Japan).[58] More details about the interpretation can be found in the original work,[59,60] as well as specifically applied to the swelling process in PNIPMAM thin films in ref 54.

Experimental Protocol. To remove already incorporated H_2O, the films were dried under a continuous nitrogen flow for 1.5 h. Subsequently, a D_2O vapor atmosphere was introduced to induce swelling of the films (4 h for ToF-NR; 15 h for FTIR) until an equilibrated state was reached. Then, the vapor atmosphere was changed to a D_2O−acetone vapor mixture with a 9:1 volume-to-volume ratio (1.5 h for ToF-NR; 5 h for FTIR).

RESULTS AND DISCUSSION

To study the solvent vapor mixture-induced contraction of PNIPMAM-based thin films with the addition of different salts, namely, $NaClO_4$ or $Mg(ClO_4)_2$, time-of-flight neutron reflectometry (ToF-NR) and Fourier transform infrared spectroscopy (FTIR) measurements are combined. Before the ToF-NR samples are subjected to the vapor flow protocol, X-ray reflectometry (XRR) and grazing incidence small-angle X-ray scattering (GISAXS) measurements are conducted to confirm a uniform vertical and lateral distribution of the salts inside the polymer film. For the in situ measurements, the films are dried under a constant nitrogen flow, followed by a solvent-vapor-induced swelling process in a D_2O vapor atmosphere until an equilibrated state is reached. The contraction of the polymer films is triggered by subsequently exposing the films to a D_2O−acetone vapor atmosphere at a 9:1 volume-to-volume ratio. Static ToF-NR measurements are conducted at the equilibrated dry, swollen, and collapsed states, while the time-resolved measurements are measured in between each static measurement, giving access to the thickness and solvent content evolution. FTIR investigations help us to comprehend the underlying molecular interactions contributing to the overall solvation mechanism. The corresponding results are discussed in the following, starting with the data collected by XRR measurements.

Distribution of Salts inside PNIPMAM Thin Films. XRR measurements are conducted of the as-prepared salt-containing PNIPMAM thin films at ambient conditions to investigate the vertical distribution of the components through the film after deposition. GISAXS measurements further provide information about the lateral salt distribution. From fits to the reflectivity curves, information about the film thickness, the scattering length density (SLD) profile, and the roughness of the films is obtained. It is noteworthy that due to the different scattering processes of X-rays compared to neutrons, materials have different SLD values in the respective measurements. On the one hand, XRR allows for a more thorough investigation of the vertical salt distribution inside the polymer films due to the enhanced contrast between the polymer and the introduced salts. On the other hand, NR allows us to investigate more thoroughly the vertical distribution and incorporation of deuterated solvent molecules inside a film since neutron SLDs are highly sensitive to isotope substitution. Figure 1 shows the measured XRR patterns of the $Mg(ClO_4)_2$- (orange) and $NaClO_4$-containing (green) PNIPMAM thin films with their corresponding fits (black) as well as the derived SLD profiles. Detailed fit results are provided in Table S1 in the Supporting Information.

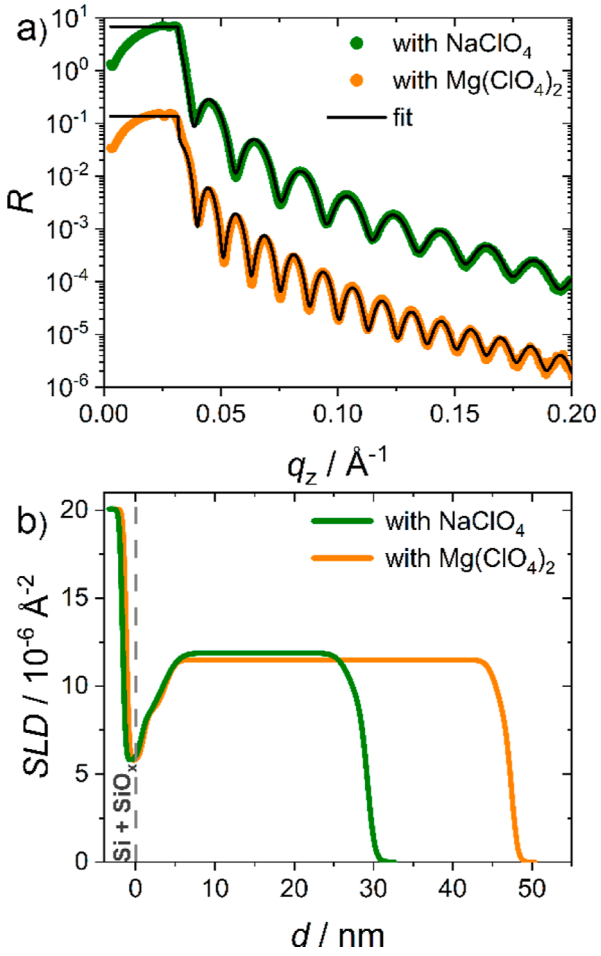

Figure 1. (a) XRR reflectivity curves of the $Mg(ClO_4)_2$- (orange) and $NaClO_4$-containing (green) PNIPMAM thin films with their corresponding fits (black) and (b) derived SLD profiles.

Both XRR reflectivity curves show pronounced Kiessig fringes even in the high q_z range, which implies the smoothness of the prepared films and therefore confirms the suitability of the salt-containing samples for ToF-NR investigation. Furthermore, from fits to the XRR data with a three-layer model consisting of, apart from a silicon layer with its native oxide layer for the substrate as well as infinite air at the top of the sample, a polymer−substrate interface, a polymer bulk layer, and a polymer−air interface, SLD profiles are observed (Figure 1b). Besides the difference in the observed film thickness, the profiles show that the shapes of the curves resemble each other. In the bulk region, a homogeneous vertical distribution of the individual salts in the polymer matrix is present, while at the interfaces, the decreased SLD values suggest either a depletion of material or the presence of already incorporated H_2O from the surrounding environment.

In addition to the information about the vertical material distribution obtained by XRR, GISAXS measurements provide information about the lateral distribution of the salts inside the thin polymer film. The 2D GISAXS data (Figure S1) and the horizontal line cuts at the Yoneda peak region of the polymer (Figure S2) are provided in the Supporting Information for a salt-free, a $Mg(ClO_4)_2$-containing, and a $NaClO_4$-containing

https://doi.org/10.1021/acs.macromol.4c02053
Macromolecules 2024, 57, 10635−10647

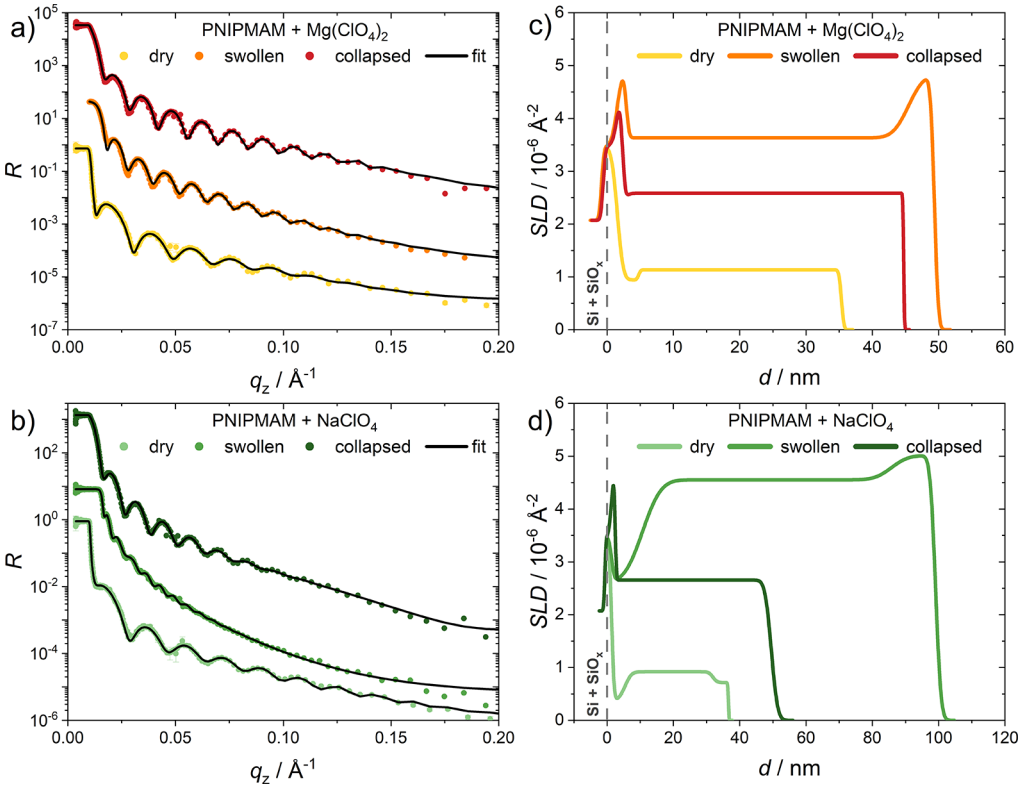

Figure 2. (a,b) Static ToF-NR reflectivity curves at the equilibrated dry (light), swollen (medium), and collapsed (dark) states with their corresponding fits (black) for the $Mg(ClO_4)_2$- (orange) and $NaClO_4$-containing (green) PNIPMAM thin films as well as (c,d) derived SLD profiles.

PNIPMAM thin film. The 2D GISAXS data of the salt-free PNIPMAM film show no pronounced scattering features besides a strong forward scattering in the resolution limit. The horizontal line cut taken at the Yoneda peak position of the polymer indicates a lack of characteristic lateral structures inside the polymer film. Thus, no characteristic variation in the lateral direction is observed, as expected for a homopolymer. Similarly, by comparison of the horizontal line cuts of the salt-containing films, no lateral features are discernible. The two line cuts show no deviations from the salt-free sample, which implies that the addition of salt does not introduce any lateral structures inside the PNIPMAM film. Therefore, a homogeneous lateral distribution of the salts inside the polymer films is confirmed.

Static Equilibrated Film States. Static ToF-NR measurements are conducted while subjecting the thin films to the experimental vapor flow protocol described in the Methods section at the equilibrated dry, swollen, and collapsed state for PNIPMAM thin films containing either $NaClO_4$ or $Mg(ClO_4)_2$ (Figure 2). The obtained reflectivity patterns are fitted by using a three-layer model as explained for the XRR data analysis, which considers different contributions throughout the sample verticals, i.e., the polymer bulk region and the potential occurrence of interfaces, besides the layers originating from the substrate. The fit parameters for the Si substrate and its native oxide layer are kept identical for each sample throughout the whole ToF-NR data analysis. Detailed results from the fits are presented in Table S2 in the Supporting Information.

Changes in the position of the critical edge and the spacing between the Kiessig fringes are observed between the individual static measurements at different equilibrated states. A shift of the critical edge toward higher q_z-values and a decrease in the spacing between the modulations are observed for the D_2O swollen films compared to the dry ones. This indicates that D_2O molecules are incorporated into the films, increasing the thickness of the whole film. Comparing the reflectivity curves obtained for the swollen and collapsed films, the opposite behavior is observed, indicating that the films contract in terms of their thickness, and the movement of the critical edge indicates the exchange to a mixture of D_2O and acetone inside the films. From fits to the reflectivity curves, SLD profiles of the PNIPMAM thin film containing either $Mg(ClO_4)_2$ or $NaClO_4$ are observed. The curves for the dry states are similar in the regard that at the bulk region, a homogeneous vertical distribution of the polymer as well as the salt is observed, which has already been confirmed with XRR measurements. Additionally, the same deviations at the interfaces, i.e., the polymer−substrate and the polymer−air interfaces, are obtained even after drying the films under a continuous nitrogen flow. Furthermore, the SLD profiles of these samples in the dry state indicate that the film thicknesses are approximately 34 nm and within 1.5 nm of each other. Comparing the SLD profiles of the individual swollen states, an increase in film thickness and an overall increase in the SLD are revealed, which is attributed to the uptake of D_2O molecules into the films. Nevertheless, the vertical solvent distribution in the films differs: while the SLD is increased at the polymer−air interface for both systems, which can be attributed to an accumulation layer of D_2O molecules on an already water saturated thin film, different behaviors are observed at the polymer−substrate interfaces. Increased SLD values at interfaces are attributed to an enrichment of D_2O molecules, which is the case for $Mg(ClO_4)_2$-containing thin

https://doi.org/10.1021/acs.macromol.4c02053
Macromolecules 2024, 57, 10635−10647

films. In the case of differing SLD behaviors at the polymer−substrate and polymer−air interfaces, the differences indicate a nonhomogeneous vertical distribution of the solvent throughout the film, as observed for the $NaClO_4$-containing PNIPMAM thin film. The change of the solvent vapor atmosphere from a D_2O to D_2O−acetone mixture leads to a decrease in the thickness and SLD of the system. Also, the D_2O enrichment layer at the polymer−air interface is depleted, while an increased SLD is still observed at the polymer−substrate interface. This indicates that the release of the solvent molecules is facilitated at the polymer−air interfaces due to the constant vapor flow, whereas attractive polar interactions between the solvent molecules and the hydrophilic surface of the silicon substrate prevent the escape of the solvent molecules. In particular, at the polymer−substrate interface, the native SiO_x oxide layer with its silanol groups is able to form hydrogen bonds with the D_2O molecules as well as with the amide functional groups of the polymer.

Kinetic Film Thickness Changes. To investigate the kinetic evolution between the equilibrated states, time-resolved ToF-NR measurements are performed, for which each reflectivity curve is measured for 5 s over 3.5 h for the swelling and 1.5 h for the collapse process. The data are fitted using a single-layer model to describe the salt-containing polymer films. Furthermore, it is ensured that the fit parameters of the static measurements at the equilibrated dry and swollen states match the respective end points of the kinetic measurements. In Figure 3, selected reflectivity curves with the respective fits (black) are shown for the $Mg(ClO_4)_2$ (orange)- and $NaClO_4$ (green)-containing PNIPMAM thin films during the swelling (light color) and collapse (dark color) processes.

The shift of the critical edge and the changes in the spacing of the Kiessig fringes resemble the findings of the static ToF-NR measurements. Furthermore, the analysis provides insights about the film thickness d (Figure 4a) and the SLD evolution (Figure 4b), as well as about the evolution of the solvent content Φ (Figure 5).

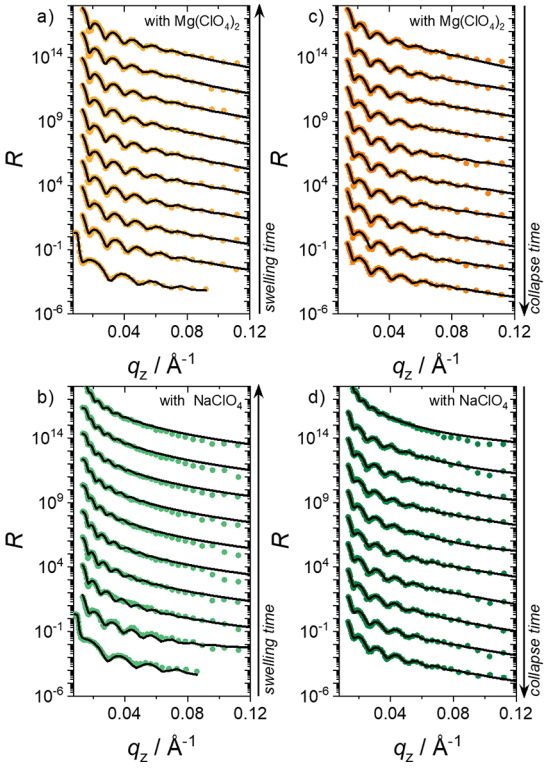

Figure 3. Selected time-resolved ToF-NR reflectivity curves for (a,b) swelling (light colors) and (c,d) collapse (dark colors) processes with their corresponding fits (black) for the $Mg(ClO_4)_2$- (orange) and $NaClO_4$-containing (green) PNIPMAM thin films. Curves are shifted along the y-axis over time, where for the swelling (a,b) reflectivity curves in intervals of 21 min and for the collapse (c,d) in intervals of 9 min are shown.

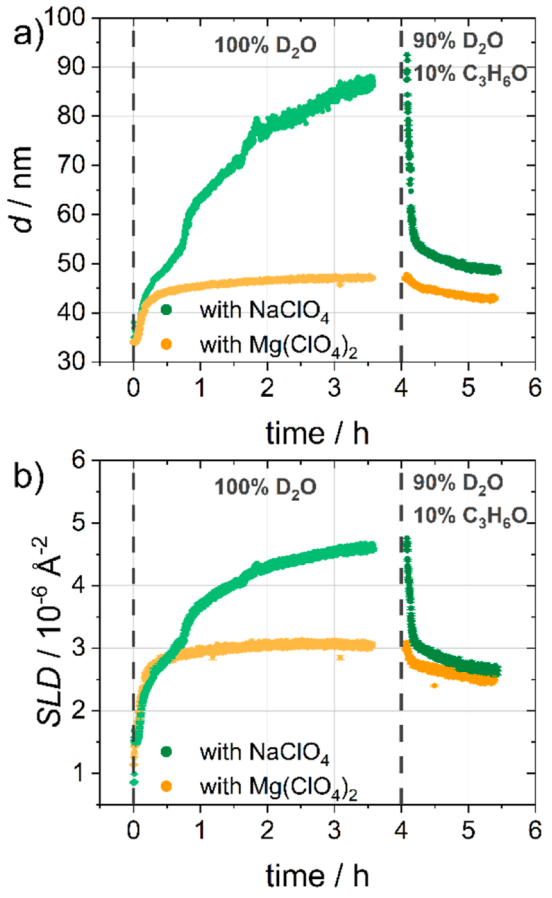

Figure 4. (a) Thickness and (b) SLD evolution over time for the swelling (light colors) and collapse (dark colors) processes of the $Mg(ClO_4)_2$- (orange) and $NaClO_4$-containing (green) PNIPMAM thin films. Dashed lines indicate changes in the vapor atmosphere, i.e., from a pure D_2O vapor atmosphere (100% D_2O) to a D_2O−acetone vapor mixture atmosphere (90% D_2O and 10% C_3H_6O).

Starting from similar initial film thicknesses in the dry states, the $Mg(ClO_4)_2$-containing PNIPMAM thin film shows a thickness increase in D_2O vapor atmosphere of 39%, whereas the $NaClO_4$-containing film reaches a much stronger thickness increase of over 177% at the same time. As demonstrated in our previous publication,[54] the swelling ability of salt-containing PNIPMAM thin films can be modified by the addition of two magnesium salts with different anions, namely, $Mg(ClO_4)_2$ and $Mg(NO_3)_2$. A detailed explanation of the interpretation of the swelling behavior of salt-containing PNIPMAM thin films is given in ref 54, whereas the focus of this work is on the contraction behavior after the exchange of the vapor atmosphere. In summary, water molecules are predominantly incorporated at the film surface until the water

https://doi.org/10.1021/acs.macromol.4c02053
Macromolecules 2024, 57, 10635−10647

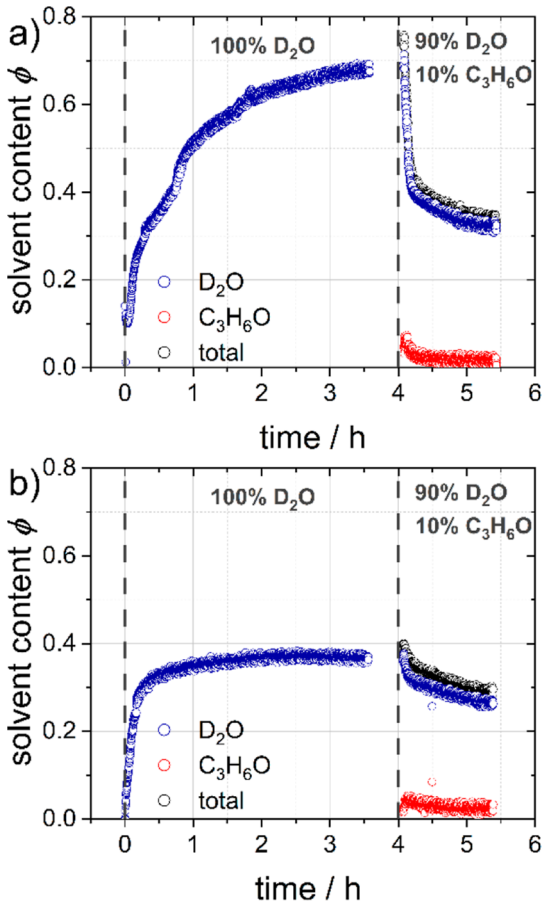

Figure 5. Solvent content evolution over time for the swelling and collapse processes for the (a) $NaClO_4$- and (b) $Mg(ClO_4)_2$-containing PNIPMAM thin films. Dashed lines indicate changes in the vapor atmosphere, i.e., from a D_2O vapor atmosphere (100% D_2O) to a D_2O−acetone solvent vapor atmosphere (90% D_2O and 10% C_3H_6O). D_2O content is indicated in blue, acetone content in red, and the total solvent content in black.

molecules diffuse into the excluded free volume in the bulk region of the polymer network. As soon as a certain amount of water is incorporated, the mobility of the polymer chains increases. This leads to a rearrangement of the polymer chains and the water network, leading to increased solvent accessibility of the polymer chains. These two main processes are assumed to be the reasons for the two-step swelling process or the different slopes of thickness evolution. It is noteworthy that for the $Mg(ClO_4)_2$-containing PNIPMAM thin films, the swelling abilities are comparable, independent of the starting film thickness ranging between 35 and 90 nm. Furthermore, this study shows that the response behavior of salt-containing PNIPMAM thin films is even more significantly enhanced by the incorporation of $NaClO_4$ compared to both Mg salts. This demonstrates that the responsiveness of PNIPMAM thin films toward a D_2O vapor atmosphere can be easily modulated by introducing specific salts.

With the introduction of the D_2O−acetone vapor mixture atmosphere in a 9:1 volume-to-volume ratio, the volume-phase transition behavior is triggered by the cononsolvency effect, resulting in an abrupt thickness decrease until an equilibrated state is reached. The system containing $Mg(ClO_4)_2$ contracted by 9%, whereas the one containing $NaClO_4$ contracted by even by 51%. Both systems shrink to a remaining swelling ratio of around 134%, which assumes a preferential solvation state of the films independent of the type of added salt. Regarding the potential of thin film systems for applications such as soft matter-based vapor-responsive nanoswitches or gas sensors, strong and fast responses of the thin films toward a change in the surrounding environment are preferred. Here, a strong change in thickness upon the exchange from a D_2O to a D_2O−acetone vapor mixture atmosphere is observed within the first 15 min. Such a rapid contraction of a salt-free polymer thin film exposed to the same conditions was observed for PMMA-*b*-PNIPMAM thin films with an initial film thickness of 140 nm.[45] However, with this study, we demonstrate that a similarly strong response is achieved by modifying PNIPMAM homopolymer thin films by the addition of salts. In Figure S3 in the Supporting Information, the thickness evolution over time for salt-free PNIPMAM homopolymer thin films exposed to the same conditions is shown.

To further investigate the influence of the observed salt dependence on the response, an analysis of the evolution of the solvent and cosolvent content over time is conducted based on the ToF-NR measurements. A detailed description of the solvent content calculation is given in the Supporting Information. In Figure 5, the calculated solvent contents $\Phi(t)$ are plotted for the $NaClO_4$ (a)- and $Mg(ClO_4)_2$ (b)-containing PNIPMAM thin films and are separated into the swelling process in a D_2O vapor atmosphere and the collapse process in a D_2O−acetone solvent vapor atmosphere. Additionally, the total solvent content for the collapse process is shown.

The PNIPMAM thin film containing $Mg(ClO_4)_2$ reaches a D_2O volume fraction of about 37% in the swollen state, whereas the $NaClO_4$-containing film reaches a value of 69%. In the case of the cononsolvency-induced contraction of the films, as the solvent vapor mixture is introduced into the system, the D_2O content inside the film immediately decreases, whereas the acetone content first increases before being again released from the film. The maximum amount of acetone uptake peaks at 5% for the $Mg(ClO_4)_2$-containing film and at 7% for the $NaClO_4$-containing film. After a delay of 15 min, the acetone content decreases and stabilizes at about 2% for both systems.

Molecular Interactions. Due to the variety of participating functional groups, the observed volume-phase transitions are governed by the interactions of the individual species. Not only do the interactions arise from electrostatic interactions, mainly originating from the contained ions, but also equally as important from the formation of hydrogen bonds between the polymer and the solvent molecules. Consequently, the magnitude of these interactions represents a sensitive probe for the progress of the volume-phase transition, which can be quantified using FTIR. Since the vibrational frequency is dependent on the bond strength of the constituting atoms, the shifts of the peak positions can be used to elucidate the relative bond strength variation over time. Collected FTIR spectra during the swelling and collapse processes are shown in Figure 6 for both salt-containing systems.

Following the discussion of the solvent contents determined by ToF-NR, the FTIR spectra confirm the overall observation that during the swelling D_2O is incorporated into the film, while during the collapse D_2O is ejected out of the system accompanied by the uptake of acetone. It should be noted that the signal at ~3360 cm^{-1}, which is attributed to the stretching vibration of H_2O, indicates the presence of residual water, which is substituted by D_2O over the course of the experiment.

https://doi.org/10.1021/acs.macromol.4c02053
Macromolecules 2024, 57, 10635−10647

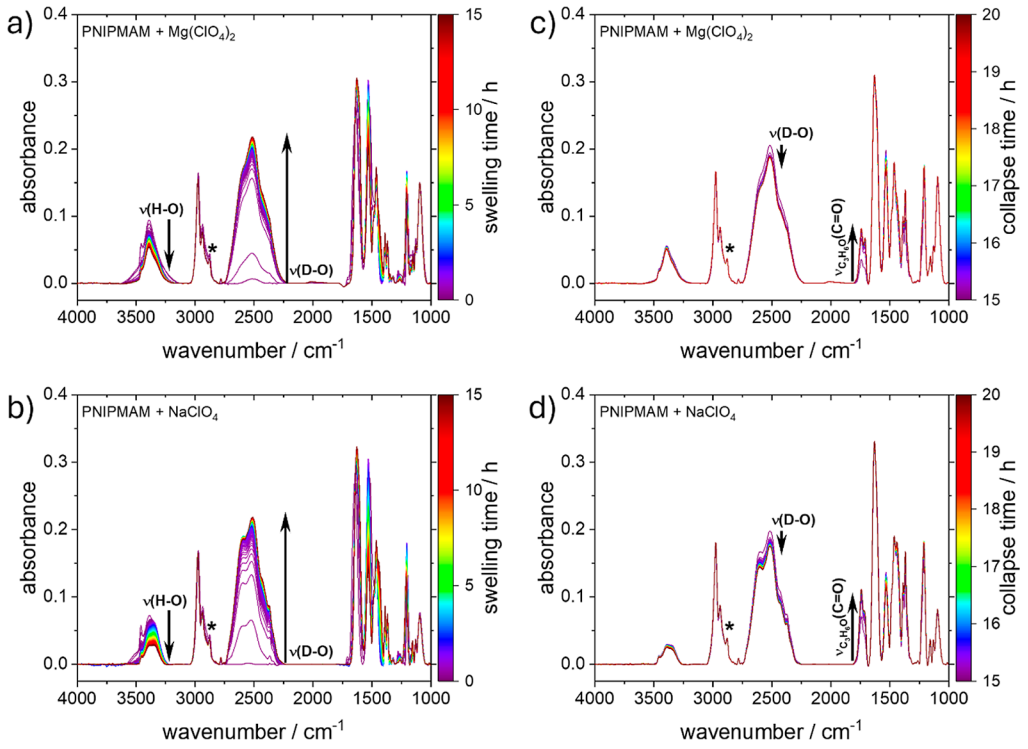

Figure 6. FTIR spectra measured during the (a,b) swelling and (c,d) collapse of a PNIPMAM film containing either $Mg(ClO_4)_2$ (top row) or $NaClO_4$ (bottom row). Normalization is done by reweighting the intensity of the $\nu_{sym}(C-H_3)$ signal in the dry state to an absorbance of 0.05. Black arrows indicate the intensity trends of the signals originating from solvent molecules over time.

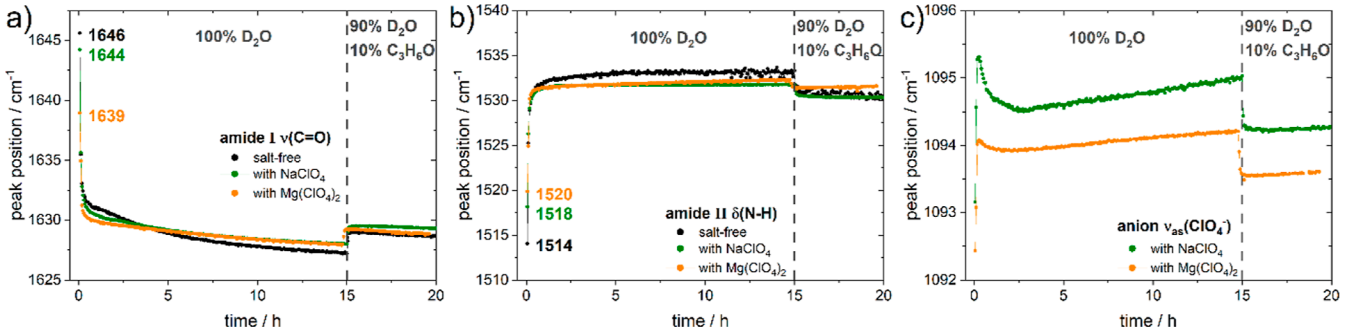

Figure 7. Time-resolved peak positions of the (a) amide I, (b) amide II, (c) $\nu_{asym}(ClO_4^-)$ signals for a PNIPMAM film containing either $Mg(ClO_4)_2$ (orange) or $NaClO_4$ (green), as well as for a salt-free reference film (black). Initial peak positions in the dry state are given in the respective colors.

To further quantify the extent of interaction changes during the transitions, the shifts of the amide I, amide II, and $\nu_{asym}(ClO_4^-)$ peaks are shown in Figure 7.

By comparing the peak positions in the initial dry states for the amide I band, it can be inferred from the red shift that ion−dipole interactions between the cations and the carbonyl groups of the polymer are formed.[61] Upon the introduction of D_2O molecules, the amide I signal shows a pronounced shift toward lower wavenumbers, indicating hydrogen bond formation, irrespective of salt addition. In contrast, the peak shifts toward higher wavenumbers when a D_2O−acetone vapor mixture is introduced. Taking into account the observation from the ToF-NR investigation that during the collapse process, D_2O is ejected from the film while acetone is incorporated, this shift can be attributed to a decreased D_2O content inside the films as well as to the inability of acetone to act as a hydrogen bond donor. However, it should be noted that the carbonyl group of acetone can still serve as a hydrogen bond acceptor. The reverse trend of the peak position shifts is observed for the amide II band since it originates mainly from a bending vibration. Furthermore, since the inorganic anion is chosen such that its absorption bands do not overlap with signals arising from the rest of the components, it can likewise be used as a probe of ion−solvent interactions. Based on the peak position shifts of the anions at the different solvent compositions, a hydration shell is formed during the D_2O uptake, while the solvation shell changes when acetone is added.

Sequence of Solvation Events. To further dissect the complex overlapping signals in the FTIR spectra, 2D FTIR correlation analysis is performed for both the swelling and collapse transitions, which is also used to infer a sequence of solvation events. The following discussion on the swelling process is restricted to key points necessary for understanding the subsequent collapse process caused by the cosolvent addition. A detailed account of the 2D FTIR correlation

https://doi.org/10.1021/acs.macromol.4c02053
Macromolecules 2024, 57, 10635−10647

analysis of the swelling process of PNIPMAM thin films containing salts was provided in earlier work.[54]

A closer inspection of the amide I signal at around 1640 cm^{-1} reveals that during the D_2O uptake, a shoulder at lower wavenumbers appears. The appearance and the further development of this shoulder are attributed to the formation of NHC═O···D-OD interactions, while the main part of the band stems from intra- or intermolecular NHC═O···H−N interactions between the polymer chains. In 2D correlation analysis, the sign of a crosspeak in the asynchronous spectrum gives information about whether the change in the signals is delayed or accelerated, respectively, to one another. In Figure 8, the crosspeak in the asynchronous spectrum between the amide I and II bands is positive (red), which—according to Noda's rules[59,60]—however, has to be interpreted as negative (blue) due to the negative sign of the crosspeak in the synchronous spectrum between the bands. Therefore, the changes in the amide I signal occur before the amide II signal evolves.

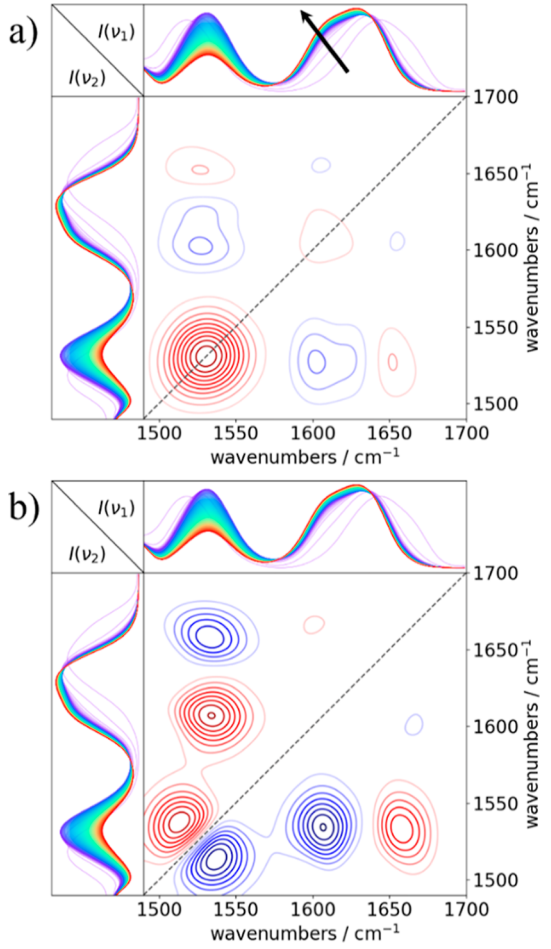

Figure 8. (a) Synchronous and (b) asynchronous 2D FTIR correlation plots in the wavenumber range between 1490 and 1700 cm^{-1} attributed to the amide I and the amide II signals of the $NaClO_4$-containing PNIPMAM film during the swelling. A positive correlation is indicated in red, and a negative correlation is indicated in blue. The black arrow indicates the formation of NHC=O···D-OD hydrogen bonds.

As the focus of this work is on the investigation of the changes in the solvation state upon the transition from a D_2O to a D_2O−acetone solvent vapor mixture atmosphere, in the following section, the 2D FTIR correlation analysis is carried out for the contracting film. Since the origin of the cononsolvency effect of polymers is still under debate,[19] which is due to the multicomponent nature of the investigated systems, the application of 2D FTIR correlation analysis is particularly attractive. Additionally, the investigation of thin films in a vapor atmosphere instead of using polymers in solution helps to decelerate the solvation process and, thus, allows us to gain further insights. By choosing a polymer-(co)solvent system with several nonoverlapping signals, in addition to using FTIR-active anions, the intricate design of the chosen system is highlighted. First, the amide signals are investigated, for which the 2D FTIR correlation plots are shown in Figure 9.

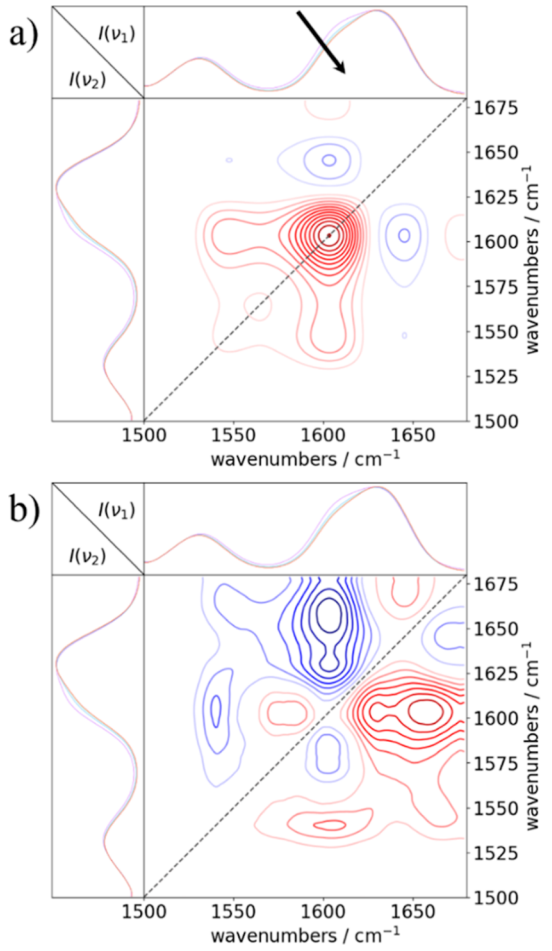

Figure 9. (a) Synchronous and (b) asynchronous 2D FTIR correlation plots in the wavenumber range between 1500 and 1680 cm^{-1} attributed to the amide I and the amide II signals of the $NaClO_4$-containing PNIPMAM film during the contraction. A positive correlation is indicated in red, and a negative correlation is indicated in blue. The black arrow indicates the depletion of NHC═O···D-OD hydrogen bonds.

The buildup of the shoulder in the amide I signal during the swelling process is attributed to NHC═O···D-OD interactions. During the exchange of vapor atmospheres, the previously incorporated D_2O is released, which is reflected by the decrease in the intensity of the shoulder, revealing that hydrogen bonds between the polymer and D_2O are perturbed.

https://doi.org/10.1021/acs.macromol.4c02053
Macromolecules 2024, 57, 10635−10647

By analyzing the correlation spectra for the amide bands during the contraction process, the order NHC═O···D-OD > NHC=O···H−*N* > amide II can be deduced, in which the first two interactions are attributed to the amide I signal. This sequence of events is the same as for the swelling process. It is believed that the introduction of acetone molecules reduces amide−D_2O interactions and that due to the contraction and solvent release, polymer−polymer interactions are increasingly formed.

To additionally elucidate cosolvent−polymer interactions, the signal arising from the carbonyl group of the acetone molecules in the range of 1680 to 1800 cm^{-1} is analyzed. Figure 10 shows the 2D FTIR correlation plots of this signal.

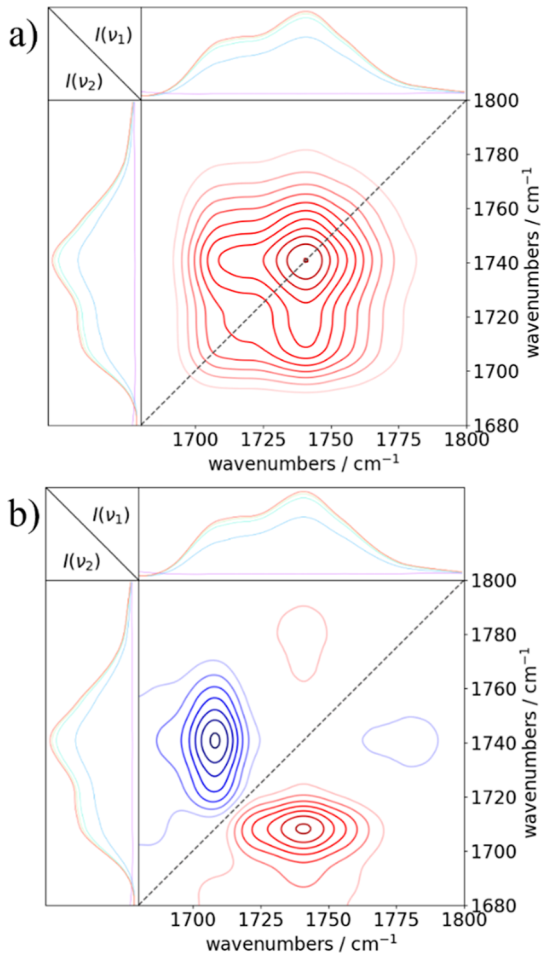

Figure 10. (a) Synchronous and (b) asynchronous 2D FTIR correlation plots in the wavenumber range between 1680 and 1800 cm^{-1} attributed to the stretching vibration of the carbonyl group of acetone for the $NaClO_4$-containing PNIPMAM film during the contraction. A positive correlation is indicated in red, and a negative correlation is indicated in blue.

A closer inspection reveals that the band consists of two individual signals. These are attributed to acetone−acetone interactions (Me_2C═O) at higher wavenumbers and acetone−amide interactions (Me_2C═O···H−N) at lower wavenumbers. Evaluation of the correlation plots reveals that acetone is first introduced into the film before acetone−amide interactions are formed. Furthermore, cross analysis between the amide and acetone signals is performed, as shown in Figure 11.

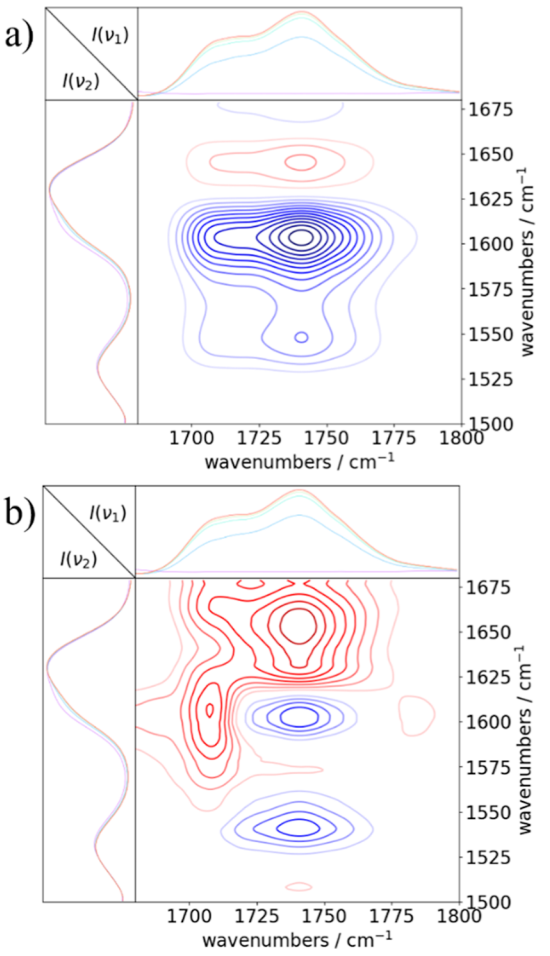

Figure 11. (a) Synchronous and (b) asynchronous cross analysis 2D FTIR correlation plots in the wavenumber range between 1680 and 1800 cm^{-1} and between 1500 and 1680 cm^{-1} for the $NaClO_4$-containing PNIPMAM film during the contraction. A positive correlation is indicated in red, and a negative correlation is indicated in blue.

The overall sequence of changes in the signals is deduced as ν(Me_2C═O) > ν(NHC═O···D-OD) > ν(Me_2C═O···H−N) > ν(NHC═O···H−N). This finding signifies that first acetone is incorporated into the films, followed by the depletion of the amide−D_2O interactions, which is accompanied by the formation of amide−acetone interactions and the formation of the again more preferred amide−amide interactions of the polymer itself. Finally, the role of the introduced anions in the solvation mechanism can be evaluated by cross-correlating the changes in the $\nu(ClO_4^-)$ signal at around 1095 cm^{-1} with the signals arising from the acetone molecules and from the amide functional groups of the polymer. Figure 12 shows the corresponding two-dimensional FTIR correlation plots.

Figure 12a,b illustrates the cross analysis between the anion and the amide signals, revealing the sequence of ν(NHC═O···D-OD) > $\nu(ClO_4^-)$ > ν(NHC═O···H−N) > amide II. Additionally, the cross analysis between the anion and the acetone signals in Figure 12c,d indicates the order of ν(Me_2C═O) > $\nu(ClO_4^-)$ > ν(Me_2C═O···H−N). In general, due to the charged nature of the anion, interactions with polar solvent molecules are preferred over the interactions with the polymer chains. Therefore, as expected, acetone molecules first change the solvation shell around the perchlorate anion before

https://doi.org/10.1021/acs.macromol.4c02053
Macromolecules 2024, 57, 10635−10647

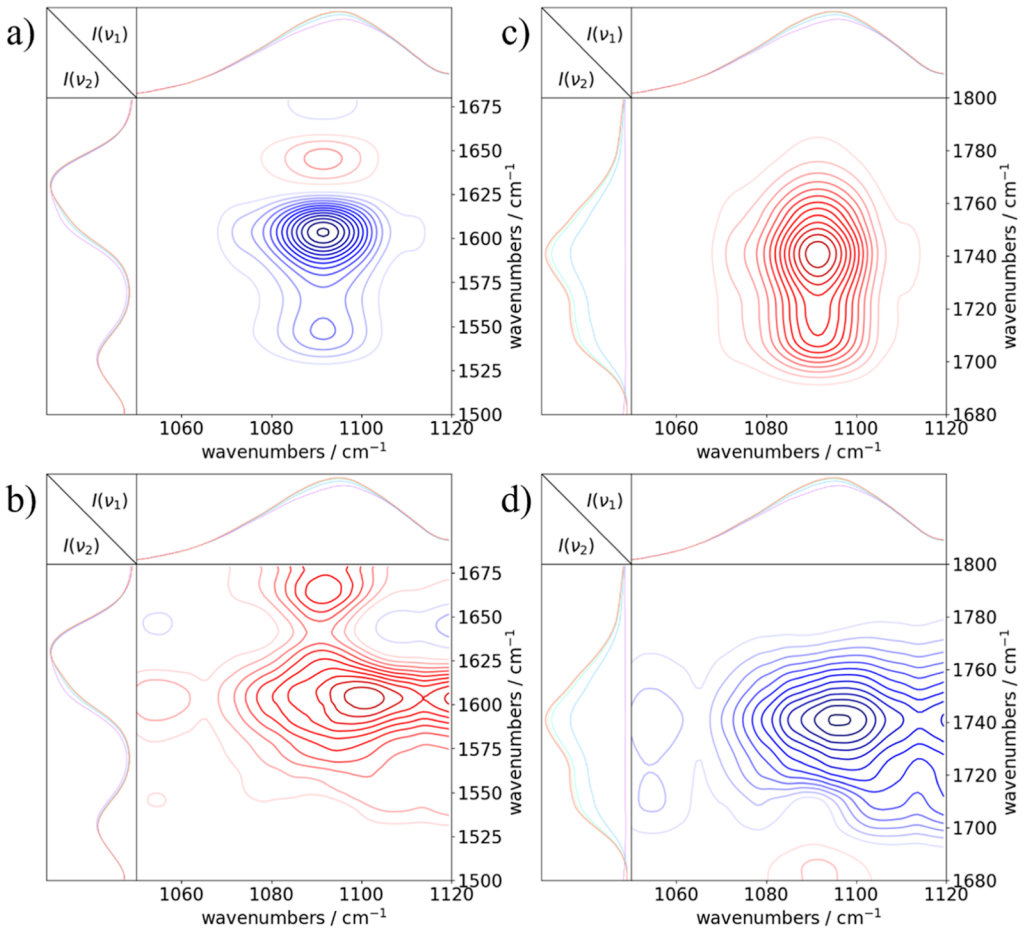

Figure 12. (a,c) Synchronous and (b,d) asynchronous cross analysis 2D FTIR correlation plots in the wavenumber range between 1050 and 1120 cm^{-1} and between 1500 and 1680 cm^{-1} and also between 1050 and 1120 cm^{-1} and between 1680 and 1800 cm^{-1} for the $NaClO_4$-containing PNIPMAM film during the contraction. A positive correlation is indicated in red, and a negative correlation is indicated in blue.

they participate in hydrogen bonding with the amide moiety. Nevertheless, the amide−D_2O interactions are also rapidly disturbed due to the strong sensitivity of the polymer toward the cosolvent. Together with the change in the solvation shell around the anion, this constitutes the first step of the contraction process. Overall, due to the incorporation of acetone molecules, the D_2O hydration shells around the polar and protic amide functional groups of the polymer, as well as around the perchlorate anions, get disturbed. Additionally, despite the formation of amide−acetone interactions, an increase in amide−amide interactions is observed, which is attributed to the contraction of the polymer films.

CONCLUSIONS

In this study, the response behavior of $NaClO_4$- or $Mg(ClO_4)_2$-containing PNIPMAM films is investigated in terms of the swelling behavior in a D_2O vapor atmosphere, as well as the subsequent contraction in a D_2O−acetone vapor mixture atmosphere, inducing a cononsolvency effect. For the as-prepared thin films, XRR and GISAXS measurements confirm the uniform vertical and lateral distribution of the introduced salts inside the polymer matrix. Static and time-resolved ToF-NR measurements enable the investigation of the solvent incorporation and reveal that the response of the films toward the different vapor atmospheres can be modulated by the type of perchlorate salt added. The $NaClO_4$-containing PNIPMAM thin films exhibit a strong film thickness increase of 177% in D_2O and a pronounced decrease of 51% in D_2O−acetone vapor atmosphere. In contrast, the $Mg(ClO_4)_2$-containing PNIPMAM thin films reach a moderate film thickness increase of 39% and a slight decrease of 9%. Investigation of the evolution of the solvent contents inside the films reveals the solvent incorporation and release processes caused by cosolvent addition. After the D_2O molecules are incorporated during the swelling process, the contraction of the films leads to a release of D_2O molecules, while the acetone concentration inside the films first builds up to 7 vol % before subsequently depleting to around 2 vol %. Furthermore, the solvation behavior is studied on a molecular level by in situ FTIR. The spectra series are analyzed by investigating the peak position shifts of signals corresponding to functional groups, which participate in the solvation events. Furthermore, the spectra are subjected to 2D FTIR correlation analysis to elucidate the sequence of solvation events. Exemplarily using the amide functional group as a probe for the solvation behavior, reveals that during the swelling process, D_2O−amide interactions are formed, which are perturbed upon the addition of acetone. During the vapor exchange, D_2O−amide interactions reduce, while acetone−amide interactions develop accompanied by amide−amide interactions, which again become favored during the contraction. A detailed understanding of the complex kinetic processes during water uptake and cosolvent-induced water release is beneficial for a fundamental knowledge-based development of polymer-based nanodevices in thin film

https://doi.org/10.1021/acs.macromol.4c02053
Macromolecules 2024, 57, 10635−10647

geometry. With proper parameter tuning, such as by salt addition, desired properties, such as an enhanced response, can be implemented for the limited set of established polymers without the need to design new polymers for a special purpose. Consequently, it is highly desirable to be able to attribute the complex response behavior of polymer thin films in the presence of salts to the properties of the involved ions and their corresponding specific ion effects in future work.

■ ASSOCIATED CONTENT

Supporting Information

The Supporting Information is available free of charge at https://pubs.acs.org/doi/10.1021/acs.macromol.4c02053.

Sample preparation for XRR, GISAXS, ToF-NR, SR, and FTIR measurements; methods information; detailed fit results for the XRR and static ToF-NR measurements; GISAXS data; solvent content calculation based on ToF-NR measurements; SR measurement of a salt-free PNIPMAM thin film; and 2D FTIR correlation plots of the FTIR spectra recorded (PDF)

■ AUTHOR INFORMATION

Corresponding Author

Peter Müller-Buschbaum − *Department of Physics, Chair for Functional Materials, Technical University of Munich, TUM School of Natural Sciences, Garching 85748, Germany;* orcid.org/0000-0002-9566-6088; Email: muellerb@ph.tum.de

Authors

Julija Reitenbach − *Department of Physics, Chair for Functional Materials, Technical University of Munich, TUM School of Natural Sciences, Garching 85748, Germany;* orcid.org/0000-0001-8142-7337

Peixi Wang − *Department of Physics, Chair for Functional Materials, Technical University of Munich, TUM School of Natural Sciences, Garching 85748, Germany;* orcid.org/0000-0002-3760-5252

Linus F. Huber − *Department of Physics, Chair for Functional Materials, Technical University of Munich, TUM School of Natural Sciences, Garching 85748, Germany;* orcid.org/0000-0002-6491-6654

Simon A. Wegener − *Department of Physics, Chair for Functional Materials, Technical University of Munich, TUM School of Natural Sciences, Garching 85748, Germany;* orcid.org/0000-0002-6508-3244

Robert Cubitt − *Institut Laue-Langevin, Grenoble 38000, France*

Dirk Schanzenbach − *Institut für Chemie, Universität Potsdam, Potsdam-Golm 14476, Germany*

André Laschewsky − *Institut für Chemie, Universität Potsdam, Potsdam-Golm 14476, Germany; Fraunhofer Institut für Angewandte Polymerforschung, Geiselbergstr. 69, Potsdam-Golm 14476, Germany;* orcid.org/0000-0003-2443-886X

Christine M. Papadakis − *Department of Physics, Soft Matter Physics Group, Technical University of Munich, TUM School of Natural Sciences, Garching 85748, Germany;* orcid.org/0000-0002-7098-3458

Complete contact information is available at: https://pubs.acs.org/10.1021/acs.macromol.4c02053

Author Contributions

The manuscript was written through contributions of all authors. All authors have given approval to the final version of the manuscript.

Notes

The authors declare no competing financial interest.

■ ACKNOWLEDGMENTS

We thank Deutsche Forschungsgemeinschaft (DFG) for financial support (LA 611/16−1, MU 1487/29-1, and PA 771/20-1). J.R. acknowledges funding through the German Ministry for Education and Research (BMBF) project "FlexiProb" (grant no. 05 K2016). P.W. acknowledges the China Scholarship Council (CSC). Institute Laue-Langevin and the neutron reflectometer D17 are acknowledged for beam time allocation and providing excellent equipment and support of measurements.

■ REFERENCES

(1) Stuart, M. A. C.; Huck, W. T. S.; Genzer, J.; Müller, M.; Ober, C.; Stamm, M.; Sukhorukov, G. B.; Szleifer, I.; Tsukruk, V. V.; Urban, M.; Winnik, F.; Zauscher, S.; Luzinov, I.; Minko, S. Emerging Applications of Stimuli-Responsive Polymer Materials. *Nat. Mater.* **2010**, *9* (2), 101−113.

(2) Roy, D.; Cambre, J. N.; Sumerlin, B. S. Future Perspectives and Recent Advances in Stimuli-Responsive Materials. *Prog. Polym. Sci.* **2010**, *35*, 278−301.

(3) Hu, L.; Zhang, Q.; Li, X.; Serpe, M. J. Stimuli-Responsive Polymers for Sensing and Actuation. *Mater. Horiz.* **2019**, *6* (9), 1774−1793.

(4) Hogan, K. J.; Mikos, A. G. Biodegradable Thermoresponsive Polymers: Applications in Drug Delivery and Tissue Engineering. *Polymer* **2020**, *211*, 123063.

(5) Xu, X.; Bizmark, N.; Christie, K. S. S.; Datta, S. S.; Ren, Z. J.; Priestley, R. D. Thermoresponsive Polymers for Water Treatment and Collection. *Macromolecules* **2022**, *55* (6), 1894−1909.

(6) Concilio, M.; Beyer, V. P.; Becer, C. R. Thermoresponsive Polymers in Non-Aqueous Solutions. *Polym. Chem.* **2022**, *13*, 6423−6474.

(7) Doberenz, F.; Zeng, K.; Willems, C.; Zhang, K.; Groth, T. Thermoresponsive Polymers and Their Biomedical Application in Tissue Engineering - A Review. *J. Mater. Chem. B* **2020**, *8*, 607−628.

(8) Ward, M. A.; Georgiou, T. K. Thermoresponsive Polymers for Biomedical Applications. *Polymers* **2011**, *3*, 1215−1242.

(9) Roy, D.; Brooks, W. L. A.; Sumerlin, B. S. New Directions in Thermoresponsive Polymers. *Chem. Soc. Rev.* **2013**, *42* (17), 7214−7243.

(10) Papadakis, C. M.; Müller-Buschbaum, P.; Laschewsky, A. Switch It Inside-out: "Schizophrenic" Behavior of All Thermoresponsive UCST-LCST Diblock Copolymers. *Langmuir* **2019**, *35* (30), 9660−9676.

(11) Fujishige, S.; Kubota, K.; Ando, I. Phase Transition of Aqueous Solutions of Poly(*N*-Isopropylacrylamide) and Poly(*N*-Isopropylmethacrylamide). *J. Phys. Chem.* **1989**, *93* (8), 3311−3313.

(12) Kotsuchibashi, Y.; Ebara, M.; Aoyagi, T.; Narain, R. Recent Advances in Dual Temperature Responsive Block Copolymers and Their Potential as Biomedical Applications. *Polymers* **2016**, *8* (11), 380.

(13) Zhao, C.; Ma, Z.; Zhu, X. X. Rational Design of Thermoresponsive Polymers in Aqueous Solutions: A Thermodynamics Map. *Prog. Polym. Sci.* **2019**, *90*, 269−291.

(14) Hofmann, C.; Schönhoff, M. Do Additives Shift the LCST of Poly(*N*-Isopropylacrylamide) by Solvent Quality Changes or by Direct Interactions? *Colloid Polym. Sci.* **2009**, *287* (12), 1369−1376.

(15) Panayiotou, M.; Garret-Flaudy, F.; Freitag, R. Co-Nonsolvency Effects in the Thermoprecipitation of Oligomeric Polyacrylamides from Hydro-Organic Solutions. *Polymer* **2004**, *45* (9), 3055−3061.

(16) Zhang, Y.; Cremer, P. S. Chemistry of Hofmeister Anions and Osmolytes. *Annu. Rev. Phys. Chem.* **2010**, *61*, 63−83.
(17) Umapathi, R.; Reddy, P. M.; Rani, A.; Venkatesu, P. Influence of Additives on Thermoresponsive Polymers in Aqueous Media: A Case Study of Poly(*N*-Isopropylacrylamide). *Phys. Chem. Chem. Phys.* **2018**, *20* (15), 9717−9744.
(18) Costa, R. O. R.; Freitas, R. F. S. Phase Behavior of Poly(*N*-Isopropylacrylamide) in Binary Aqueous Solutions. *Polymer* **2002**, *43* (22), 5879−5885.
(19) Bharadwaj, S.; Niebuur, B. J.; Nothdurft, K.; Richtering, W.; van der Vegt, N. F. A.; Papadakis, C. M. Cononsolvency of Thermoresponsive Polymers: Where We Are Now and Where We Are Going. *Soft Matter* **2022**, *18* (15), 2884−2909.
(20) Henschel, C.; Schanzenbach, D.; Laschewsky, A.; Ko, C. H.; Papadakis, C. M.; Müller-Buschbaum, P. Thermoresponsive and Co-Nonsolvency Behavior of Poly(*N*-Vinyl Isobutyramide) and Poly(*N*-Isopropyl Methacrylamide) as Poly(*N*-Isopropyl Acrylamide) Analogs in Aqueous Media. *Colloid Polym. Sci.* **2023**, *301* (7), 703−720.
(21) Yong, H.; Sommer, J. U. Cononsolvency Effect: When the Hydrogen Bonding between a Polymer and a Cosolvent Matters. *Macromolecules* **2022**, *55* (24), 11034−11050.
(22) Mukherji, D.; Marques, C. M.; Kremer, K. Smart Responsive Polymers: Fundamentals and Design Principles. *Annu. Rev. Condens. Matter Phys.* **2020**, *11*, 271−299.
(23) Kyriakos, K.; Philipp, M.; Silvi, L.; Lohstroh, W.; Petry, W.; Müller-Buschbaum, P.; Papadakis, C. M. Solvent Dynamics in Solutions of PNIPAM in Water/Methanol Mixtures - A Quasi-Elastic Neutron Scattering Study. *J. Phys. Chem. B* **2016**, *120* (20), 4679−4688.
(24) Liu, B.; Wang, J.; Ru, G.; Liu, C.; Feng, J. Phase Transition and Preferential Alcohol Adsorption of Poly(*N*,*N*-Diethylacrylamide) Gel in Water/Alcohol Mixtures. *Macromolecules* **2015**, *48* (4), 1126−1133.
(25) Heyda, J.; Muzdalo, A.; Dzubiella, J. Rationalizing Polymer Swelling and Collapse under Attractive Cosolvent Conditions. *Macromolecules* **2013**, *46* (3), 1231−1238.
(26) Tanaka, F.; Koga, T.; Kojima, H.; Xue, N.; Winnik, F. M. Preferential Adsorption and Co-Nonsolvency of Thermoresponsive Polymers in Mixed Solvents of Water/Methanol. *Macromolecules* **2011**, *44* (8), 2978−2989.
(27) Sun, S.; Wu, P. Role of Water/Methanol Clustering Dynamics on Thermosensitivity of Poly(*N*-Isopropylacrylamide) from Spectral and Calorimetric Insights. *Macromolecules* **2010**, *43* (22), 9501−9510.
(28) Zhang, G.; Wu, C. The Water/Methanol Complexation Induced Reentrant Coil-to-Globule-to-Coil Transition of Individual Homopolymer Chains in Extremely Dilute Solution. *J. Am. Chem. Soc.* **2001**, *123* (7), 1376−1380.
(29) Hao, J.; Cheng, H.; Butler, P.; Zhang, L.; Han, C. C. Origin of Cononsolvency, Based on the Structure of Tetrahydrofuran-Water Mixture. *J. Chem. Phys.* **2010**, *132* (15), 154902.
(30) Mukherji, D.; Marques, C. M.; Kremer, K. Polymer Collapse in Miscible Good Solvents Is a Generic Phenomenon Driven by Preferential Adsorption. *Nat. Commun.* **2014**, *5*, 4882.
(31) Tanaka, F.; Koga, T.; Winnik, F. M. Temperature-Responsive Polymers in Mixed Solvents: Competitive Hydrogen Bonds Cause Cononsolvency. *Phys. Rev. Lett.* **2008**, *101* (2), 028302.
(32) Bischofberger, I.; Calzolari, D. C. E.; Trappe, V. Co-Nonsolvency of PNiPAM at the Transition between Solvation Mechanisms. *Soft Matter* **2014**, *10* (41), 8288−8295.
(33) Kreuzer, L. P.; Lindenmeir, C.; Geiger, C.; Widmann, T.; Hildebrand, V.; Laschewsky, A.; Papadakis, C. M.; Müller-Buschbaum, P. Poly(Sulfobetaine) versus Poly(*N*-Isopropylmethacrylamide): Co-Nonsolvency-Type Behavior of Thin Films in a Water/Methanol Atmosphere. *Macromolecules* **2021**, *54* (3), 1548−1556.
(34) Zhang, Q.; Hoogenboom, R. Polymers with Upper Critical Solution Temperature Behavior in Alcohol/Water Solvent Mixtures. *Prog. Polym. Sci.* **2015**, *48*, 122−142.
(35) Osaka, N.; Shibayama, M. Pressure Effects on Cononsolvency Behavior of Poly(*N*-Isopropylacrylamide) in Water/DMSO Mixed Solvents. *Macromolecules* **2012**, *45* (4), 2171−2174.
(36) Ihara, D.; Higaki, Y.; Yamada, N. L.; Nemoto, F.; Matsuda, Y.; Kojio, K.; Takahara, A. Cononsolvency of Poly[2-(Methacryloyloxy)-Ethyl Phosphorylcholine] in Ethanol-Water Mixtures: A Neutron Reflectivity Study. *Langmuir* **2022**, *38* (17), 5081−5088.
(37) Backes, S.; Krause, P.; Tabaka, W.; Witt, M. U.; Mukherji, D.; Kremer, K.; Von Klitzing, R. Poly(*N*-Isopropylacrylamide) Microgels under Alcoholic Intoxication: When a LCST Polymer Shows Swelling with Increasing Temperature. *ACS Macro Lett.* **2017**, *6* (10), 1042−1046.
(38) Chen, Q.; Kooij, E. S.; Sui, X.; Padberg, C. J.; Hempenius, M. A.; Schön, P. M.; Vancso, G. J. Collapse from the Top: Brushes of Poly(*N*-Isopropylacrylamide) in Co-Nonsolvent Mixtures. *Soft Matter* **2014**, *10* (17), 3134−3142.
(39) Yong, H.; Bittrich, E.; Uhlmann, P.; Fery, A.; Sommer, J. U. Co-Nonsolvency Transition of Poly(*N*-Isopropylacrylamide) Brushes in a Series of Binary Mixtures. *Macromolecules* **2019**, *52* (16), 6285−6293.
(40) Geiger, C.; Reitenbach, J.; Kreuzer, L. P.; Widmann, T.; Wang, P.; Cubitt, R.; Henschel, C.; Laschewsky, A.; Papadakis, C. M.; Müller-Buschbaum, P. PMMA-*b*-PNIPAM Thin Films Display Cononsolvency-Driven Response in Mixed Water/Methanol Vapors. *Macromolecules* **2021**, *54* (7), 3517−3530.
(41) Ko, C. H.; Wastian, P.; Schanzenbach, D.; Müller-Buschbaum, P.; Laschewsky, A.; Papadakis, C. M. Dynamic Behavior of Poly(*N*-Isopropylmethacrylamide) in Neat Water and in Water/Methanol Mixtures. *Langmuir* **2024**, *40*, 15150−15160.
(42) Tokarev, I.; Minko, S. Stimuli-Responsive Hydrogel Thin Films. *Soft Matter* **2009**, *5* (3), 511−524.
(43) White, E. M.; Yatvin, J.; Grubbs, J. B.; Bilbrey, J. A.; Locklin, J. Advances in Smart Materials: Stimuli-Responsive Hydrogel Thin Films. *J. Polym. Sci., Part B: Polym. Phys.* **2013**, *51* (14), 1084−1099.
(44) Ko, C. H.; Claude, K. L.; Niebuur, B. J.; Jung, F. A.; Kang, J. J.; Schanzenbach, D.; Frielinghaus, H.; Barnsley, L. C.; Wu, B.; Pipich, V.; Schulte, A.; Müller-Buschbaum, P.; Laschewsky, A.; Papadakis, C. M. Temperature-Dependent Phase Behavior of the Thermoresponsive Polymer Poly(*N*-Isopropylmethacrylamide) in an Aqueous Solution. *Macromolecules* **2020**, *53* (16), 6816−6827.
(45) Geiger, C.; Reitenbach, J.; Henschel, C.; Kreuzer, L. P.; Widmann, T.; Wang, P.; Mangiapia, G.; Moulin, J. F.; Papadakis, C. M.; Laschewsky, A.; Müller-Buschbaum, P. Ternary Nanoswitches Realized with Multiresponsive PMMA-*b*-PNIPMAM Films in Mixed Water/Acetone Vapor Atmospheres. *Adv. Eng. Mater.* **2021**, *23* (11), 2100191.
(46) Kouřilová, H.; Hanyková, L.; Spěváček, J. NMR Study of Phase Separation in D_2O/Ethanol Solutions of Poly(*N*-Isopropylmethacrylamide) Induced by Solvent Composition and Temperature. *Eur. Polym. J.* **2009**, *45* (10), 2935−2941.
(47) Alenichev, I.; Sedláková, Z.; Ilavský, M. Swelling and Mechanical Behavior of Charged Poly(*N*-Isopropylmethacrylamide) and Poly(*N*-Isopropylacrylamide) Networks in Water/Ethanol Mixtures. Cononsolvency Effect. *Polym. Bull.* **2007**, *58* (1), 191−199.
(48) Wang, P.; Geiger, C.; Kreuzer, L. P.; Widmann, T.; Reitenbach, J.; Liang, S.; Cubitt, R.; Henschel, C.; Laschewsky, A.; Papadakis, C. M.; Müller-Buschbaum, P. Poly(Sulfobetaine)-Based Diblock Copolymer Thin Films in Water/Acetone Atmosphere: Modulation of Water Hydration and Co-Nonsolvency-Triggered Film Contraction. *Langmuir* **2022**, *38*, 6934−6948.
(49) Gerlach, G.; Guenther, M.; Hartling, T. Hydrogel-Based Chemical and Biochemical Sensors - A Review and Tutorial Paper. *IEEE Sens. J.* **2021**, *21* (11), 12798−12807.
(50) Bloksma, M. M.; Bakker, D. J.; Weber, C.; Hoogenboom, R.; Schubert, U. S. The Effect of Hofmeister Salts on the LCST Transition of Poly(2-Oxazoline)s with Varying Hydrophilicity. *Macromol. Rapid Commun.* **2010**, *31* (8), 724−728.
(51) Zhang, Y.; Furyk, S.; Bergbreiter, D. E.; Cremer, P. S. Specific Ion Effects on the Water Solubility of Macromolecules: PNIPAM and

https://doi.org/10.1021/acs.macromol.4c02053
Macromolecules 2024, 57, 10635−10647

the Hofmeister Series. *J. Am. Chem. Soc.* **2005**, *127* (41), 14505−14510.
(52) Zhang, Y.; Furyk, S.; Sagle, L. B.; Cho, Y.; Bergbreiter, D. E.; Cremer, P. S. Effects of Hofmeister Anions on the LCST of PNIPAM as a Function of Molecular Weight. *J. Phys. Chem. C* **2007**, *111* (25), 8916−8924.
(53) Heyda, J.; Dzubiella, J. Thermodynamic Description of Hofmeister Effects on the LCST of Thermosensitive Polymers. *J. Phys. Chem. B* **2014**, *118* (37), 10979−10988.
(54) Reitenbach, J.; Geiger, C.; Wang, P.; Vagias, A.; Cubitt, R.; Schanzenbach, D.; Laschewsky, A.; Papadakis, C. M.; Müller-Buschbaum, P. Effect of Magnesium Salts with Chaotropic Anions on the Swelling Behavior of PNIPMAM Thin Films. *Macromolecules* **2023**, *56*, 567−577.
(55) Nelson, A. J.; Prescott, S. W. Refnx: Neutron and X-Ray Reflectometry Analysis in Python. *J. Appl. Crystallogr.* **2019**, *52*, 193−200.
(56) Widmann, T.; Kreuzer, L. P.; Mangiapia, G.; Haese, M.; Frielinghaus, H.; Müller-Buschbaum, P. 3D Printed Spherical Environmental Chamber for Neutron Reflectometry and Grazing-Incidence Small-Angle Neutron Scattering Experiments. *Rev. Sci. Instrum.* **2020**, *91* (11), 113903.
(57) Sears, V. F. Neutron Scattering Lengths and Cross Sections. *Neutron News* **1992**, *3* (3), 26−37.
(58) Morita, S. 2Dpy https://github.com/shigemorita/2Dpy (accessed Nov 23, 2023).
(59) Noda, I. Two-Dimensional Infrared Spectroscopy. *J. Am. Chem. Soc.* **1989**, *111* (21), 8116−8118.
(60) Noda, I.; Dowrey, A. E.; Marcott, C. Recent Developments in Two-Dimensional Infrared (2D IR) Correlation Spectroscopy. *Appl. Spectrosc.* **1993**, *47* (9), 1317−1323.
(61) Mahalakshmi, M.; Selvanayagam, S.; Selvasekarapandian, S.; Moniha, V.; Manjuladevi, R.; Sangeetha, P. Characterization of Biopolymer Electrolytes Based on Cellulose Acetate with Magnesium Perchlorate ($Mg(ClO_4)_2$) for Energy Storage Devices. *J. Sci. Adv. Mater. Devices* **2019**, *4* (2), 276−284.

https://doi.org/10.1021/acs.macromol.4c02053
Macromolecules 2024, 57, 10635−10647